Quantum paraelectric and induced ferroelectric states in SrTiO3

Joachim Hemberger, Michael Nicklas, R. Viana, Peter Lunkenheimer, Alois Loidl, R. Böhmer

Angaben zur Veröffentlichung / Publication details:

Hemberger, Joachim, Michael Nicklas, R. Viana, Peter Lunkenheimer, Alois Loidl, and R. Böhmer. 1996. "Quantum paraelectric and induced ferroelectric states in SrTiO3." *Journal of Physics: Condensed Matter* 8 (25): 4673–90. https://doi.org/10.1088/0953-8984/8/25/021.

Quantum paraelectric and induced ferroelectric states in $SrTiO_3$

J Hemberger†, M Nicklas†, R Viana†, P Lunkenheimer†, A Loidl† and R Böhmer‡

† Institut für Festkörperphysik, Technische Hochschule Darmstadt, D-64289 Darmstadt, Germany

‡ Institut für Physikalische Chemie, Johannes Gutenberg-Universität, D-55099 Mainz, Germany

Abstract. Nominally pure $SrTiO_3$ has been studied by dielectric spectroscopy using small (linear regime) as well as large electrical fields (non-linear regime) up to 1 kV mm^{-1}. In addition measurements of the specific heat and its field-dependent contribution have been carried out. The field dependence of the dielectric constant and the specific heat can be well described by the transverse Ising Hamiltonian including tunnelling and external field terms. It gives evidence for the existence of polar clusters at low temperatures which are supposed to be associated with the quantum paraelectric state below $T_q \approx 37$ K in accord with recent free-energy calculations. The low-field third-harmonic susceptibility which measures the polar correlations exhibits anomalies near T_q. At high fields an aligned domain state is induced. These results as well as those on the remanent polarization and the dielectric loss have allowed us to deduce a complex E, T-phase diagram. The assignment of the various phases is discussed in connection with the recent proposal of the appearance of a macroscopic quantum state.

1. Introduction

In the perovskites $SrTiO_3$ and $KTaO_3$ the low-temperature paraelectric state is stabilized by quantum fluctuations, i.e. zero-point motions or tunnelling excitations of the dipolar degrees of freedom [1]. This means that in the absence of internal or external perturbations electrical order cannot be established down to the lowest temperatures. Recently the question has been raised by Müller *et al* of whether these quantum fluctuations are a superposition of incoherent modes, or whether, in analogy to the case of superfluid helium, the coupling of the lowest transverse acoustic and the soft mode gives rise to a *coherent* quantum paraelectric state in $SrTiO_3$ [2]. These conjectures were stimulated by the observation of an anomaly in paramagnetic resonance experiments, indicative of a phase transition near 37 K in this material.

Subsequent to this remarkable proposal a number of investigations, including ones using the methods of light [3, 4] and neutron scattering [5], sound dispersion [6] and attenuation [7], EXAFS [8] and dielectric spectroscopy [9], have confirmed the existence of anomalies possibly due to a phase transition that takes place near 35 K. Several observations, in particular those associated with domain properties and the T-dependence of phonon modes, are compatible with the supposed coherence of the low-temperature state of the pure crystal. It is thought that the quantum paraelectric state can easily be destroyed by introducing substitutional defects into the lattice, which act as pinning centres for the polar modes

[10, 11]. Ferroelectric order can also be produced by the application of external electrical [12, 13, 14] and mechanical [15] stresses which couple to the polar modes.

In this article we have used dielectric spectroscopy in order to study the dynamics of the electrically active modes over a broad frequency and temperature range. By variation of the externally applied fields we are able to study the system not only under `zero-field' conditions, but also in the state of induced ferroelectricity. The latter is achieved by application of large ac as well as dc electrical fields. A field–temperature phase diagram is obtained from the dielectric results. The phase boundary separating the quantum paraelectric and the induced ferroelectric regions is reproduced quantitatively by a simple mean-field Ising model, which can also be used to describe the field-dependent contribution of the specific heat.

2. Tunnelling and large electrical fields: predictions from an Ising model

The dielectric susceptibility of quantum paraelectrics like $SrTiO_3$ deviates from simple Curie-law behaviour at low temperatures due to quantum mechanical tunnelling effects. Extending Slater's mean-field theory, Barret [16] derived an expression which accounted well for the observed low-field susceptibility [1, 12]. Incorporation of Barret's result in a phenomenological Landau type of expansion of the free energy allowed Hegenbarth [13, 17] to describe quantitatively the transition from the quantum paraelectric to the external field-driven ferroelectric state. The explicit field dependence of the susceptibility is often accounted for by using its Taylor expansion in powers of the external electric field. In strongly interacting and/or random (e.g. slightly doped) systems superparaelectric clusters may form which recently have been described using a Langevin type of formula [18]. In order to treat the electrical field dependence of the susceptibility, the interactions of the dipole moments, as well as the quantum mechanical effects in a unified framework, it has been suggested [14] that one should consider the following Hamiltonian:

$$\mathcal{H} = -\Omega \sum_i S_i^x - \frac{1}{2} \sum_{i,j} J_{ij} S_i^z S_j^z - 2\mu E \sum_i S_i^z. \tag{1}$$

Here the dipolar degrees of freedom are schematically represented by the Ising spin operators $\hat{S} = (S^x, S^y, S^z)^\dagger$. The first two terms in equation (1) constitute the well known transverse Ising model [19]. Here the exchange constants J_{ij} couple the longitudinal pseudo-spin components S^z while the transverse ones appear together with the tunnelling integral Ω. The effect of the externally applied field E is taken into account by the term $-2\mu E \sum_i S_i^z$. Here μ denotes the strength of the dipole moments, i.e. the magnitude of coupling to the electrical field. In the mean-field approximation (MFA) equation (1) can be written as [19]

$$\mathcal{H}^{MFA} = \frac{\partial \langle \mathcal{H} \rangle}{\partial \langle \hat{S} \rangle} \hat{S} = -\boldsymbol{H} \hat{S} \tag{2}$$

with the generalized molecular field

$$\boldsymbol{H} = \left(\Omega, 0, \sum_{i,j} J_{ij} \langle S^z \rangle + 2\mu E \right)^\dagger \tag{3}$$

where the brackets $\langle \cdots \rangle$ denote thermal averaging. This Hamiltonian is easily seen to be solved by

$$\langle \boldsymbol{S} \rangle = \frac{1}{2} \frac{\boldsymbol{H}}{H} \tanh \left(\frac{H}{2k_B T} \right) \tag{4}$$

with $H = |\boldsymbol{H}| = \sqrt{\Omega^2 + (J_0\langle\hat{S}\rangle + 2\mu E)^2}$, and the effective coupling constant $J_0 = \sum_j J_{ij}$. The longitudinal component of this relation leads to the expression

$$\langle S^z\rangle = \frac{1}{2}\frac{J_0\langle S^z\rangle + 2\mu E}{H}\tanh\left(\frac{H}{2k_BT}\right) \tag{5}$$

which is to be solved self-consistently. The measured dielectric susceptibility

$$\chi(E) = \lim_{\Delta E\to 0}\frac{P(E) - P(E+\Delta E)}{\varepsilon_0\,\Delta E} \tag{6}$$

can then be calculated from the macroscopic polarization

$$P = 2n\mu\langle S^z\rangle \tag{7}$$

where n is the density of dipole moments. In the limit of small fields one obtains

$$\chi = \frac{nk_B^2\mu^2}{(\Omega/2)\coth(\Omega/2k_BT) - J_0/4} \tag{8}$$

which is identical with the formula given by Barret [16] if one identifies T_0 with $J_0/4k_B$ and T_Ω with Ω/k_B. The Barret equation is useful for the description of quantum paraelectrics, since it yields a strongly temperature-dependent susceptibility for $\Omega > J_0/2$ which however saturates for lower T. This saturation of the susceptibility is a hallmark of the quantum paraelectric state and vanishes if the external field is strong enough. In this induced ferroelectric case a maximum in χ at a temperature T_c occurs, indicating the formation of the ordered state.

The dependence of T_c on electrical field E and effective coupling constant J_0 as predicted by equations (5)–(7) is shown in figure 1 in a three-dimensional representation. These results are a generalization of those obtained previously [13, 19].

From the macroscopic polarization one also can obtain the change in the free energy of a homogeneous dielectric sample with volume V upon application of a uniform electrical field [20]:

$$\Delta F = F_E - F_0 = -\frac{1}{2}VEP. \tag{9}$$

From the general thermodynamic relation $\mathrm{d}F = -S\ \mathrm{d}T - p\ \mathrm{d}V + \mathrm{d}W_{el}$ we obtain the following expression for the entropy:

$$S = -\left(\frac{\partial F}{\partial T}\right)_{V,E}.$$

This allows us to calculate the field-dependent contribution of entropy and specific heat:

$$\Delta S = S_E - S_0 = \frac{1}{2}VE\left(\frac{\partial P}{\partial T}\right)_{V,E} \tag{10}$$

and

$$\Delta C = T\left(\frac{\partial\,\Delta S}{\partial T}\right)_{V,E} = \frac{1}{2}VET\left(\frac{\partial P^2}{\partial^2 T}\right)_{V,E}. \tag{11}$$

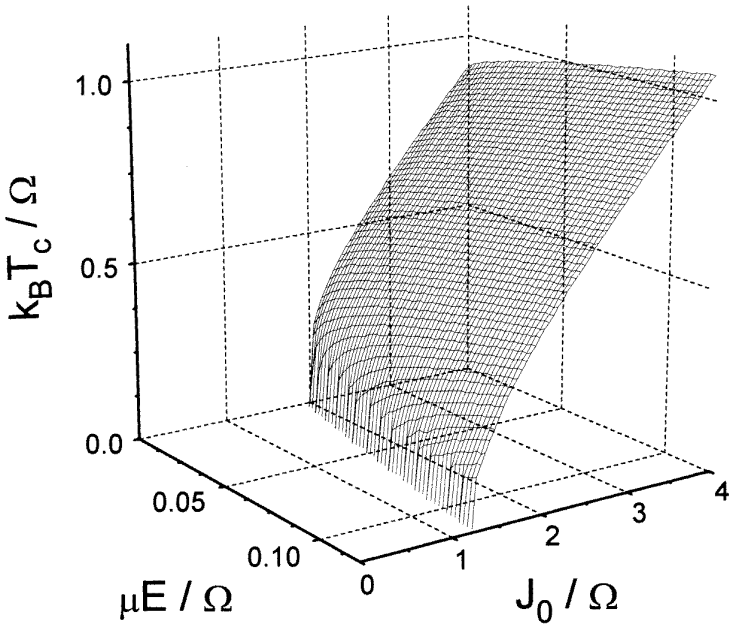

Figure 1. The transition temperature T_c yielded by the transverse Ising Hamiltonian as a function of the external field E and the effective coupling constant J_0. Both parameters are normalized to the tunnelling integral Ω. T_c has been calculated from the maximum of the susceptibility as given by equations (5)–(7).

3. Experimental details

3.1. Sample preparation

The nominally pure samples of $SrTiO_3$ were obtained commercially from Crystal Co. and Goodfellow Co. Their stoichiometry and purity were checked by electron microprobe measurements using wavelength-dispersive techniques. We found that the fraction of alkaline (earth) ions was below 400 ppm. In particular the concentration of Ca^{2+} ions was below 200 ppm. Additional measurements were conducted on samples containing either Cr or Ni impurities in various concentrations up to the 1000 ppm level. In order to study the effects of surface layers several samples were examined before as well as after etching in orthophosphoric acid. No qualitative changes of the dielectric properties could be found. Thin crystal slabs with typical dimensions of $10 \times 5 \times 1$ mm^3 and oriented along the cubic [110] axis were prepared for the dielectric measurements. For the measurements of the field-dependent heat capacity, samples of size $10 \times 10 \times 3$ mm^3 were used. Gold electrodes were sputtered onto 7 nm Cr layers covering the large faces of the crystals. No attempts were made to obtain monodomain samples. The standard specific heat measurements were performed on a larger sample (about 5 g).

3.2. Dielectric measurements

Most of the dielectric measurements were carried out using a modified Sawyer–Tower circuit [21], in which the sample was connected in series with a reference capacitor whose

capacitance was larger by at least a factor of 1000 than that of the sample [22]. The voltage across the reference capacitor is a measure of the polarization P in the sample, while the voltage across the sample determines the macroscopic field E. An electrometer amplifier, with an input impedance $\geqslant$200 TΩ, was used as impedance transformer enabling the detection of $P(E)$-cycles in the mHz regime. The $P(E)$-data were recorded using digital lock-in techniques and were analysed with standard Fourier-analysis algorithms [22]. Three different experimental procedures were used in the course of this work: (i) a symmetric, harmonically alternating electric field with a large amplitude E_0 was used for the determination of the higher-order terms of the dielectric susceptibility; (ii) a small ac component superimposed on a dc bias field was utilized to determine $\varepsilon(T, E_{Bias})$ via an analysis of the local derivative of $P(E_{Bias})$; and (iii) in order to detect effects of thermoremanent polarization a cycle of zero-field cooling (ZFC), field heating (FH), field cooling (FC) and zero-field heating (ZFH) was applied. During each step the external field was held constant and the polarization was measured while ramping the sample temperature at a constant rate. Rates of 1 and 2 K min^{-1} were used but no discernible differences were found.

Some additional data were taken using the impedance analysers 4284A and 4191A from Hewlett–Packard.

3.3. Heat capacity measurements

The measurements of the heat capacity were conducted in a non-commercial adiabatic Nernst calorimeter. The specific heat was measured in a temperature range from 3 K to 50 K. The field-dependent measurements were performed in electric fields up to 500 V mm^{-1} using a high-voltage amplifier. The sample heater and the temperature sensor were mounted on the grounded side of the crystal platelet to increase the insulation to its high-voltage side. To determine $c_p(E)$ and $c_p(E = 0)$ in the same conditions of the sample environment, c_p was measured subsequently with and without an applied electrical field within the same measurement series. As a consequence of the extremely small field-dependent changes of the heat capacity, the experimental data were smoothed before the heat capacity difference $\Delta c_p = c_p(E) - c_p(E = 0)$ was calculated.

4. Results and discussion

4.1. The linear dielectric response of $SrTiO_3$

The complex dielectric constant of $SrTiO_3$, as measured at small signal levels (excitation level $<$1 V_{rms}), is shown in figure 2. The real part, shown as $1/\varepsilon'$ versus T exhibits a Curie–Weiss type of behaviour at high temperatures and saturates at a relatively high level of $\varepsilon' \approx 12\,000$. It is noted, however, that in monodomain samples the dielectric permittivity can be significantly larger [1]. Otherwise ε' is almost frequency independent and quite featureless. Consequently the losses in the sample are very small. As shown in the lower frame of figure 2, $\tan\delta$ is always smaller than 0.003; however, several features are remarkable. At temperatures near and below the structural cubic-to-tetragonal phase transition at $T_c = 105$ K [23], frequency-dependent losses are seen. These are connected with the dynamics of domain walls in the antiferrodistortive state and have similarly been observed in elastic measurements [5]. It is noted that even above T_c a precursor of this phenomenon could be detected [24]. Also in harmony with the elastic measurements, an increase of the loss is seen to occur near 40 K. Nes *et al* have ascribed this phenomenon

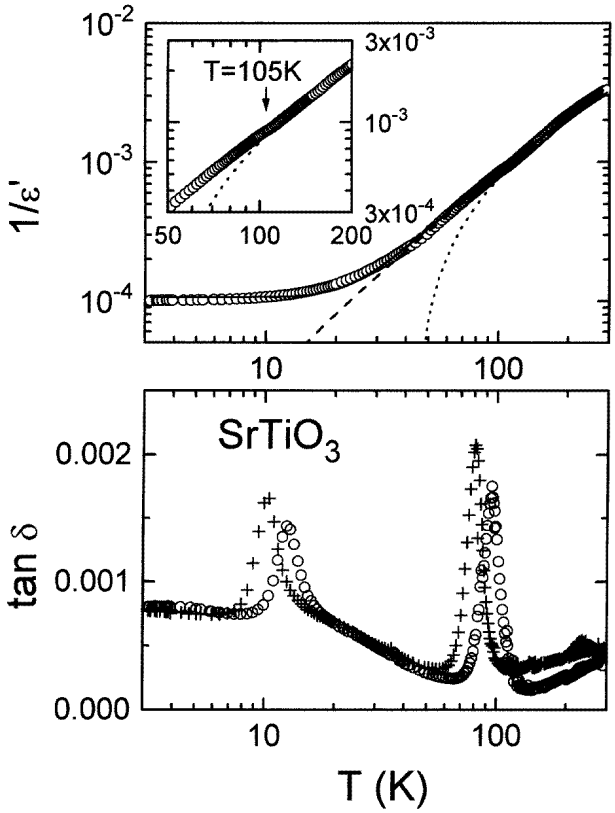

Figure 2. The inverse dielectric permittivity ε' versus T plotted on a double-logarithmic scale (upper frame) and the loss factor $\tan\delta$ versus T on a logarithmic scale (lower frame). The data refer to the frequencies 85.7 kHz (○) and 5.5 kHz (+). The dotted line is the result of a fit using the Curie–Weiss law with $\Theta \approx 45$ K. Here only temperatures above 120 K are considered. The dashed line is calculated using $\varepsilon' \sim T^{-\gamma}$ with $\gamma = 1.33$ in the temperature range 40 K $< T <$ 100 K. The solid line represents the Barret formula with $T_0 = 34$ K and $T_\Omega = 84$ K. The inset shows a `blow up' of the area around the structural phase transition at $T = 105$ K.

to the onset of domain wall scattering [7]. The dielectric loss peaks seen near 10 K have been ascribed to solitonic excitations between mutually tilted domains within the coherent quantum phase [9]. The domains characterize regions of coherently flipped dipole moments.

The temperature dependence of the loss processes is summarized in figure 3 where we show $\varepsilon''(\log\nu)$ and have plotted the most probable relaxation frequencies ν_P taken from the loss maxima in an Arrhenius representation. The high-temperature relaxation can be described by $\nu_P = 0.2$ THz $\times \exp(-1400\ \mathrm{K}/T)$. For the low-temperature process considerable curvature is noted in the representation of figure 3. Such a curvature may be due to tunnelling excitations and has similarly been observed in Ca-doped $SrTiO_3$ [25] and in $SrTiO_{2-x}$ [26]. The shape of the loss peak indicates the presence of a distribution of relaxation times with pronounced contributions from slow dipolar modes. This kind of behaviour has variously been described by strophoidal [27] and Lacroix–Béné [28] types of function. Unfortunately, due to the background correction necessary in order to obtain the data presented in the inset of figure 3, a detailed analysis of the shape of the loss peaks is

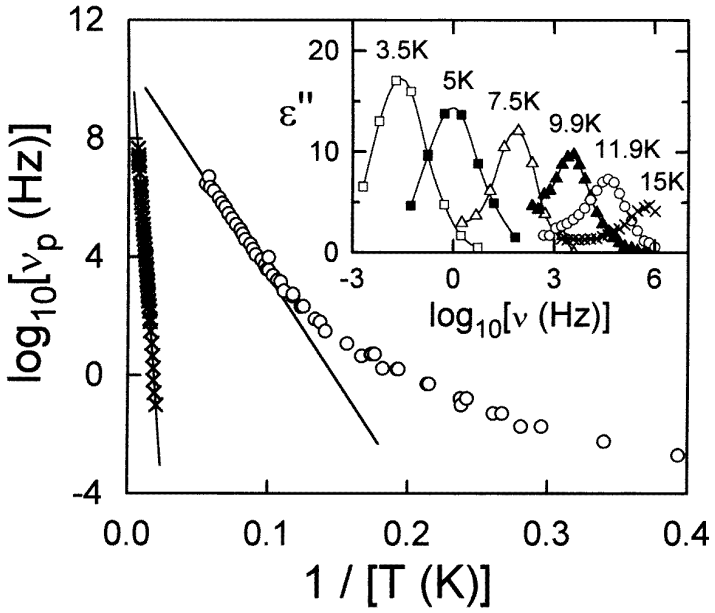

Figure 3. An Arrhenius plot for the high-temperature (×) and the low-temperature relaxations (○) in $SrTiO_3$. The straight lines represent Arrhenius behaviour. The inset shows the background-corrected dielectric loss $\varepsilon''(\log_{10}\nu)$ in the quantum paraelectric state. The most probable relaxation rate has been determined from the centre of the dielectric loss peaks. The solid lines in the inset are drawn to guide the eyes.

not advisable.

Interestingly the dielectric loss features look qualitatively similar in the Cr- and Ni-doped $SrTiO_3$ samples studied in this work. We find that the dispersion strength of this process apparently does not vary with concentration in a systematic manner. This observation suggests that a defect-related mechanism is unlikely. On the other hand a recent study by Bidault *et al* [29] on a number of nominally pure and intentionally doped perovskites has provided some evidence that the low-temperature loss phenomena are of polaronic origin.

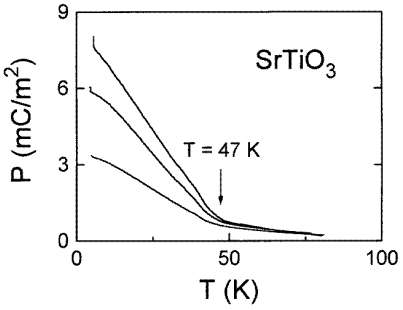

Figure 4. Thermoremanent polarization of $SrTiO_3$ after cooling down in static bias fields of (from bottom to top) 100, 300 and 500 V mm^{-1} on a linear temperature scale. A significant change of slope for $T = 47 \pm 2$ K can be detected in all curves.

According to these authors the loss peaks signal the localization of these excitations probably on residual defect states, e.g. oxygen vacancies. Bidault *et al* conjecture that this mechanism should be operative also in pure $SrTiO_3$. On the other hand they note that while in $SrTiO_3$ the loss peaks show up near 10 K (cf. the lower frame of figure 2), the process is found in the vicinity of 40 K for all other perovskites investigated by them. Hence it appears that further studies are required before a firm conclusion concerning the microscopic origin of the relaxational modes in $SrTiO_3$ can be drawn. Returning to the real part, which is plotted in the upper frame of figure 2 as $1/\varepsilon'$ versus temperature, one notes immediately that a simple Curie–Weiss relationship $\varepsilon \sim (T - \Theta)^{-\gamma}$ with $\gamma = 1$ is inadequate to describe the data over the entire temperature range. Taking into account the high-T data ($T > 120$ K) only, a Θ of about 37 ± 3 K is deduced in accord with previous reports [1, 30]. From the low-T permittivity ($T < 100$ K) a Curie–Weiss temperature $\Theta = 20$ K is estimated. A fit of similar quality is possible with $\Theta = 0$, if the exponent is used as an adjustable parameter. Then $\gamma = 1.33$ is found. This exponent is significantly larger than the classical mean-field exponent of $\gamma = 1$ but can be well rationalized in terms of the mode-coupling approach discussed by Müller and Burkhard [1]. As has been noted previously [31], the best description over an extended temperature range is achieved using the Barret formula, equation (8). The solid line in figure 2 has been calculated using $J_0/k_B = 4T_0 = 137$ K and $\Omega/k_B = 84$ K. Since the relatively heavy titanium ion is thought to be associated with tunnelling modes, Ω appears to be quite large, and indicates that a single soft-mode picture is inadequate for the description of the quantum fluctuations.

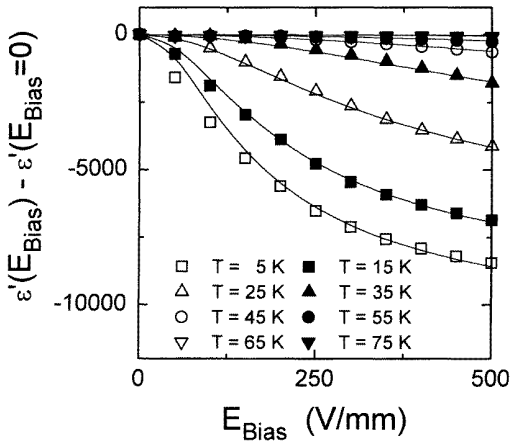

Figure 5. The field-dependent contribution to the real part of the dielectric constant ε' for various temperatures. The measurements were performed using a harmonic field component of $E_0 = 30$ V mm^{-1} at $\nu = 100$ mHz. The solid lines are fits obtained using equations (5)–(7), setting $J_0/k_B = 145$ K and with $\Omega = 87$ K fixed for all temperatures.

4.2. Metastable polarization

To gain further insights into the nature of the low-temperature state, we have attempted not only to study the low-frequency excitations under equilibrium conditions but also far away from equilibrium. Such a state can easily be obtained by cooling $SrTiO_3$ in the presence of an externally applied field E_x. In the subsequent heating run, which was carried out in zero electric field, the thermoremanent polarization (TRP) was measured. Figure 4 shows the

results obtained for different values of E_x and using heating rates of 1–2 K min^{-1}. It is noted that no significant rate dependence could be detected. The TRP shows a low-temperature value which depends on E_x. Upon heating, the TRP decreases continuously and falls off more precipitously, reaching very small values near 45–50 K for all E_x. Hence, the dipolar degrees of freedom which have been frozen in the FC cycle thaw in this temperature range, in a manner that is surprisingly similar to what is observed in orientational glasses [32, 33]. This provides experimental evidence that short-range order of the dipolar degrees of freedom exists already at approximately 50 K. However, we have to admit that in the interpretation of these results one has to be cautious. The metastable polarization is measured in a quasistatic experiment. The relaxation time of the domains of the tetragonal phase amounts to 10 s at 50 K (see figures 3 and 7). Hence we cannot fully exclude the possibility that this anomaly is connected with the multidomain state.

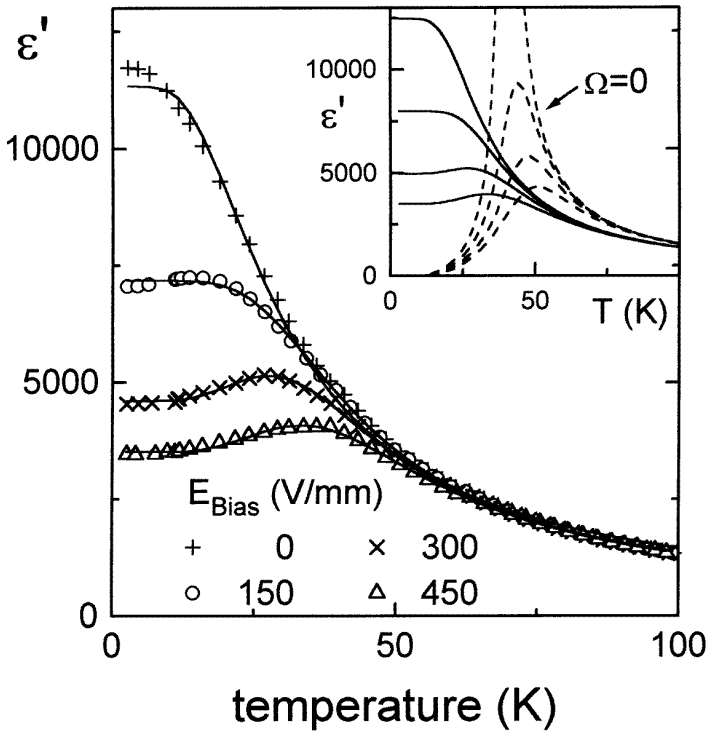

Figure 6. The real part of the temperature-dependent dielectric constant ε' for various bias fields E_{Bias}. The measurements were performed using an ac field component of $E_{ac} = 30$ V mm^{-1} and a frequency of $\nu = 100$ mHz. The solid lines are fits obtained using equations (5)–(7). The inset may illustrate the influence of the tunnelling effects represented by Ω. The solid lines show calculations with the set of parameters yielded by the fitting procedure ($J_0/k_B = 145$ K, $\Omega/k_B = 87$ K, $n = 3.6 \times 10^{26}$ m^{-3}, $\mu = 12$ eÅ). The dashed lines in the inset are calculated with the same parameters but $\Omega = 0$.

4.3. The field-dependent dielectric constant

The dielectric constant as measured in large dc electrical fields with an excitation field of 30 V mm^{-1} and at a frequency of 100 mHz is shown in figure 5 as $\Delta\varepsilon = \varepsilon'(E_{Bias}) - \varepsilon'(0)$

versus E_{Bias}. The data were taken sweeping the bias field E_{Bias} from 0 V mm^{-1} to 500 V mm^{-1} at constant temperatures. Figure 5 shows that at high temperatures, ε' is almost independent of E_{Bias}, while a significant field-induced decrease of $\Delta\varepsilon$ develops for temperatures $T < 50$ K. It is useful to plot the data explicitly as a function of temperature, as is done in figure 6. Figure 6 reveals that a maximum in $\varepsilon'(T)$ develops if $E_{Bias} \geqslant 150$ V mm^{-1}. This maximum in the permittivity, which shows pronounced shifts with E_{Bias}, signals the onset of induced ferroelectric order. The inset in figure 6 shows the model calculations that describe the experimental results (dashed lines) and compares them to those calculated for the same set of parameters but with zero quantum energy (solid lines). It is clearly demonstrated that in $SrTiO_3$, even in high electrical fields, quantum fluctuations play a important role.

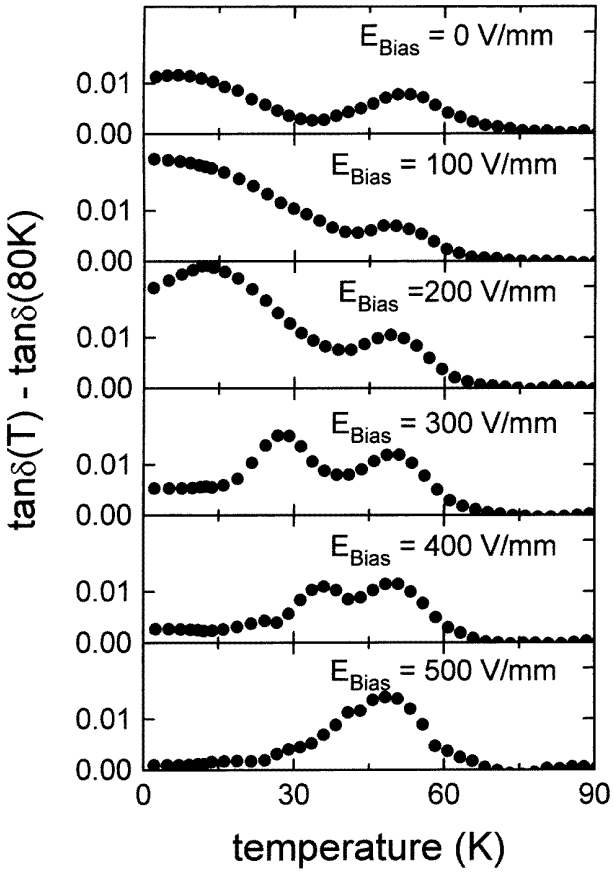

Figure 7. The loss factor tan δ as function of temperature for various bias fields. The measurements were performed using an ac field component of $E_{ac} = 30$ V mm^{-1} and a frequency of $\nu = 100$ mHz.

The loss tangent as measured under various bias fields at a frequency of 100 mHz is shown in figure 7. Near 50 K a peak shows up for all E_{Bias} which is the low-frequency counterpart of the peaks seen in figure 2 near 80 K. The field independence of these peaks is compatible with their elastic origin. More interesting is the field dependence of the low-temperature loss. The absorption in the quantum paraelectric regime can easily

be suppressed by the application of electrical fields and for $E > 200$ V mm^{-1} a loss peak emerges which shows an E-dependence like that found for the maxima seen in the permittivity $\varepsilon'(E, T)$.

For a qualitative description of the data presented in figures 5 and 6, we have used the Ising model presented in section 2. We have simultaneously fitted the temperature and the field dependences of the dielectric permittivity using equations (5)–(7). The results of this calculation are represented as solid lines in figures 5 and 6. A convincing description of the entire set of data is obtained except for for low temperatures and fields. Deviations from the description with the simple Ising model are expected to appear if excitations, like e.g. cluster modes or coherent quantum tunnelling effects, which are not included in equation (1), show up. The parameters yielded by the fitting procedure are $J_0/k_B = 145$ K, $\Omega/k_B = 87$ K, $n = 3.6 \times 10^{26}$ m^{-3}, and $\mu = 12\ e$Å. The mean interaction corresponds to a critical temperature $T_0 = J_0/4 = 36$ K, in the notation of Barret [16]. The other parameters cannot be understood easily in the framework of a single-ion picture. The large dipole moment together with the low density n (as compared to the nominal density of Ti^{4+} ions, $n_0 = 1.6 \times 10^{28}$ m^{-3}) suggests that the fluctuating dipolar entities form clusters containing a large number of unit cells. Currently it is an open question whether the notion of the existence of clusters can also help to explain the relatively high tunnelling frequency of $\nu = k_B\Omega/h = 1.8$ THz.

It is interesting to note that via a free-energy expansion for $SrTiO_3$ [15] the squared polarization $\langle P^2\rangle = (n\mu)^2 = 4.5 \times 10^{-3}$ (C m^{-2})^2 of the clusters can be used to estimate the deviation $\delta\Phi$ of the staggered rotation angle Φ of the oxygen octahedra from their theoretically expected value [34]. From the free-energy expansion parameters Hehlen *et al* estimated that $\delta\Phi/\langle\Phi\rangle = \alpha\langle P^2\rangle$ with $\alpha = 8.3$ (C m^{-2})$^{-2}$ [35]. Using the $\langle P^2\rangle$ as obtained in the present study one finds $\delta\Phi/\langle\Phi\rangle = 0.04$ in perfect agreement with the value inferred from the EPR study performed by Müller *et al* (see [2, 34, 35]).

4.4. The non-linear dipolar susceptibility

The non-linear susceptibility can also be determined by application of a sinusoidally varying electrical field E_{ac} with amplitudes large enough to excite higher harmonics.

The non-linear susceptibility χ_3 probes ferroelectric pair correlations between dipole moments [36]. Typical raw data for this type of experiment are presented in figure 8, where we have plotted $P(E)$-curves measured at 10 K and 65 K, for three amplitudes. At both temperatures, for small E_{ac}, linear and loss-free behaviour is found. For field amplitudes $\geqslant 200$ V mm^{-1} only for the low temperature, slim but lossy hysteresis loops, i.e. indications for induced remanent polarization, are observed. The magnitude of the non-linear susceptibility χ_3 as deduced from the $P(E)$-data is shown in figure 9. For large fields the behaviour of the non-linear susceptibility can easily be understood since the temperature dependence of χ_1 is known (figure 2). This is because in mean-field theory, in the vicinity of a ferroelectric transition, the relation $\chi_3 \sim \chi_1^4$ should be valid [25]. As demonstrated in the inset of figure 9, such a behaviour can be confirmed for $SrTiO_3$. At fields below 200 V mm^{-1} deviations from this relation show up, and for field amplitudes in this range a distinct minimum can be detected close to 33 K. Focusing on the 50 V mm^{-1} curve, we propose the following explanation: below about 60 K, χ_3 increases due to the growth of FE correlations. The change in the behaviour of χ_3 indicates the change in the character of the quantum fluctuations from incoherent to coherent. The drastic decrease below $T \approx 45$ K reflects incoherent quantum fluctuations, which suppress FE correlations. The recovery of χ_3 below 33 K provides experimental evidence that FE correlations grow

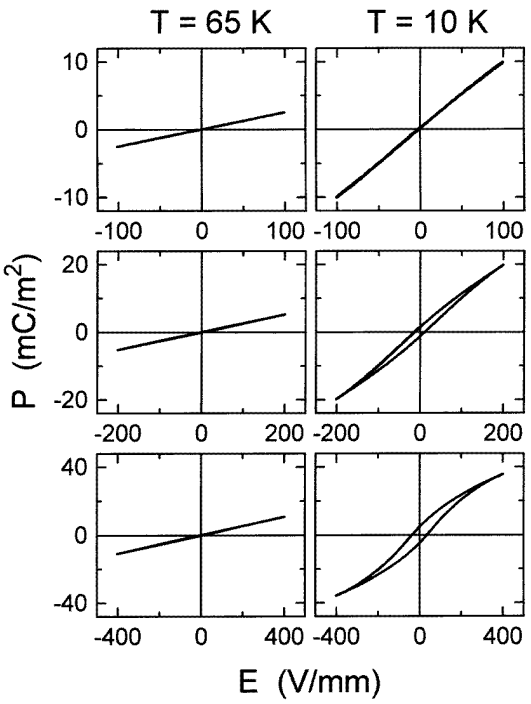

Figure 8. Hysteresis loops for field amplitudes of 100 V mm^{-1}, 200 V mm^{-1}, and 400 V mm^{-1}, obtained temperatures of 65 K and 10 K. The measurements were performed at $\nu = 1$ Hz.

again due to the onset of a coherent quantum state, which according to our interpretation is the coherent flipping of polar clusters via tunnelling transitions. For fields $E > 200$ V, induced ferroelectric correlations dominate the non-linear response.

The temperature of this anomaly in $\chi_3(T)$ exactly corresponds to the anomaly in the temperature dependence of the Debye–Waller factor (DWF) of the oxygen ions as observed by EXAFS spectroscopy [8]. A maximum in the DWF indicates maximum disorder in accordance with our interpretation.

Very recently the third-order dielectric susceptibility has been calculated for a quantum paraelectric system including quadrupolar interactions by Martoňák and Tosatti [37]. Close to T_q they found an anomaly in χ_3 in close analogy to the experimental results. The anomaly was interpreted as a remainder of the first-order ferroelectric phase transition in a quantum-frustrated system. Further experiments and theoretical work will be necessary to study the relationship between this theoretically postulated quadrupolar coupling and a possible quantum coherence at low temperatures.

4.5. The field-dependent heat capacity

In order to investigate the influence of the polar order behaviour we examined the specific heat of $SrTiO_3$ in the temperature regime below $T = 50$ K for different electric field strengths 0 V mm^{-1} $\leqslant E \leqslant$ 500 V mm^{-1}. The zero-field measurements are shown in figure 10.

The inset shows c_p as a function of temperature. We carefully studied the temperature regime 20 K $< T <$ 50 K, but no anomaly due to a phase transition could be detected.

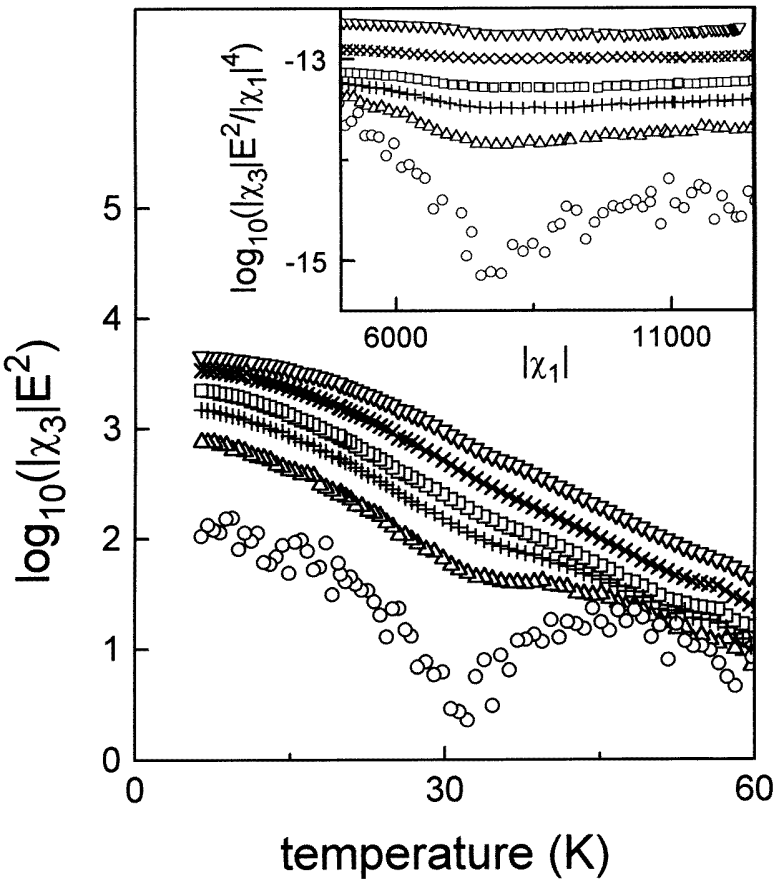

Figure 9. A semilogarithmic representation of the non-linear dielectric susceptibility $|\chi_3|E^2$ of $SrTiO_3$ as a function of temperature, for the electric fields $E_0 = 50$ V mm^{-1} (○), 100 V mm^{-1} (△), 150 V mm^{-1} (+), 200 V mm^{-1} (□), 300 V mm^{-1} (×), 450 V mm^{-1} (▽). The inset shows the same data plotted as $\log_{10}(|\chi_3|E^2/|\chi_1|^4)$ versus $|\chi_1|$.

In various scenarios that have been elucidated by Martoňák and Tosatti [38] to describe a possible low-temperature phase transition in $SrTiO_3$, a clear anomaly should show up in the specific heat in this temperature range.

In the main frame of figure 10 we plotted $\log_{10}(c_p/T^3)$ versus the logarithm of temperature. These data are in perfect agreement with early results obtained by Hegenbarth (see [39]). A significant excess peak dominates the shape of the curve showing c_p/T^3 in the temperature range 20 K $\leqslant T \leqslant$ 40 K. This glasslike excess peak is typical for dielectrics of the ABO_3 perovskite group and can be described by Einstein terms due to low-lying optic modes. Interestingly, in the crossover regime between the linear term, $c_p \propto T$, that evolves for $T < 2$ K [39], and the region of the excess heat capacity, the specific heat follows $c_p/T^3 \propto T^{-\kappa}$ ($\kappa \approx \frac{1}{4}$) in a limited temperature range. This behaviour points towards additional contributions to the specific heat from excitations of unknown origin which dominate in the range 2 K $< T <$ 10 K.

Finally we present the main results of our measurements of the heat capacity at different electrical fields and compare them with the model calculations. Figure 11 shows the

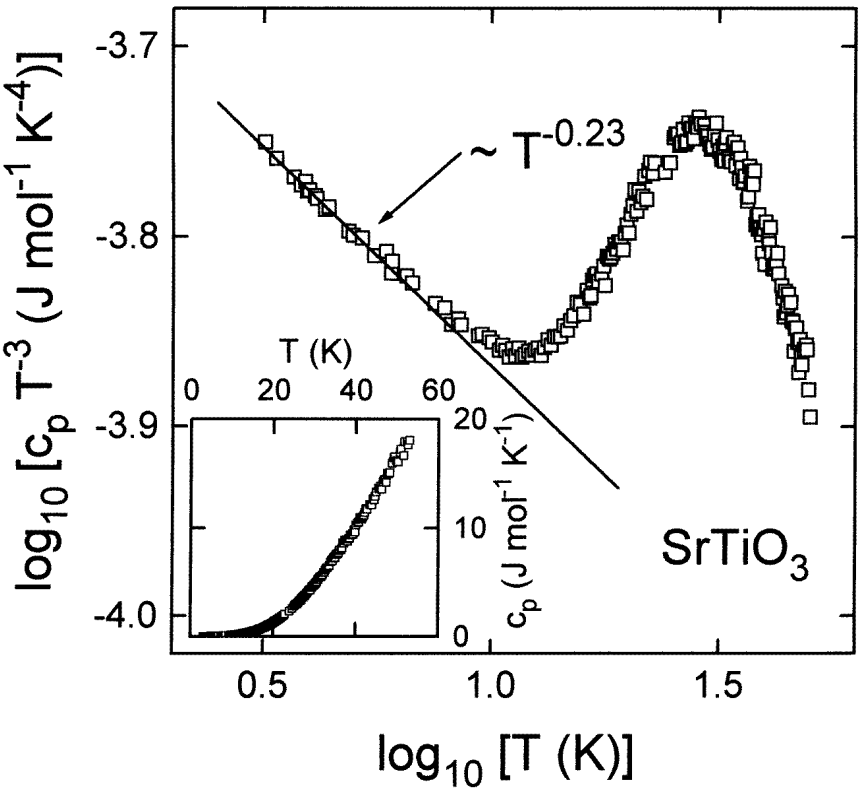

Figure 10. $\log_{10}(c_p/T^3)$ on a logarithmic temperature scale. The straight solid line is a fit using $c_p/T^3 \propto T^{\kappa}$ in the temperature range below 3 K $\leqslant T \leqslant$ 8 K. The temperature behaviour is in accordance with measurements by Henning and Hegenbarth [39]. The inset shows the raw c_p-data on the same temperature scale.

experimental results in comparison with the theoretical calculations (left-hand frames). The upper panel shows the incremental heat capacity $\Delta c_p = c_p(E) - c_p(E = 0)$ for fields of 200 V mm^{-1} and 500 V mm^{-1} at low temperatures. Qualitatively the main observations are rather well described within our model. The same is true if the excess entropy is calculated from Δc_p (lower panels). The decrease of the heat capacity due to the onset of induced FE order is nicely reproduced. However, experimentally additional contributions show up around 10 K which correspond to the power-law behaviour of c_p/T^3 (figure 10) and are not described in the simple Hamiltonian (equation (1)).

Our specific heat data can also be compared to measurements of the electrocaloric effect in $SrTiO_3$ single crystals which were performed by Hegenbarth [17, 40]. Applying an electric field E to a dielectric medium will result in a change of temperature ΔT, provided that the sample is kept under adiabatic conditions. For comparison with the model calculations we use the simple assumption that this temperature change is comparable to the change of entropy ΔS associated with the application of the field under isothermal conditions via the relation $c_p\,\Delta T \approx -T\,\Delta S$ [41]. The solid line in figure 12 shows $\Delta c_p = T\,\partial\,\Delta S/\partial T$ calculated from Hegenbarth's data (inset) and the zero-field specific heat data of this work. The experimental results correspond qualitatively to the model calculations (dashed lines).

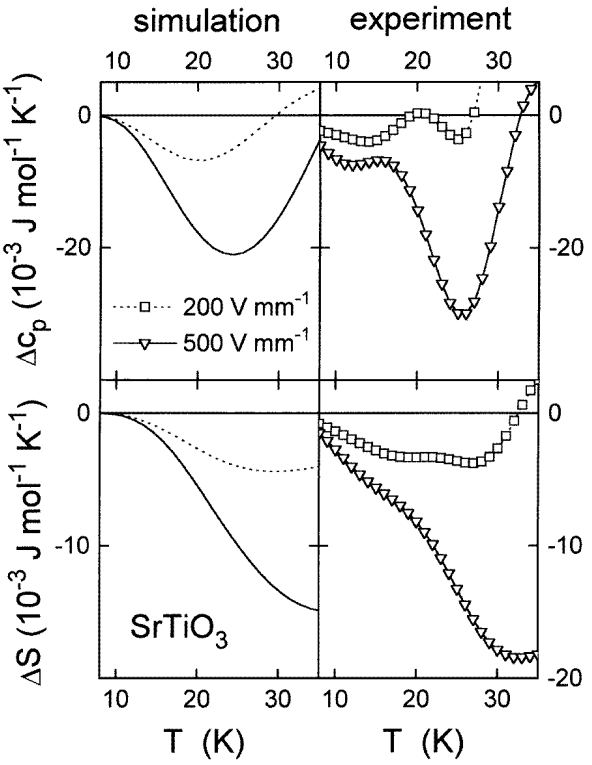

Figure 11. The temperature dependence of the contribution to the heat capacity Δc_p and the entropy ΔS due to the electric fields $E = 200$ V mm^{-1} and $E = 500$ V mm^{-1}. The frames on the left-hand side show calculations using equations (10) and (11) with the parameter set yielded by the dielectric measurements of figure 6.

4.6. The E,T-phase diagram

From the various results obtained in this work, we have deduced the temperature versus electrical field phase diagram shown in figure 13. Coming from high temperatures the transition line near $T \approx 47$ K separates ergodic and non-ergodic states as is evident from the FC/ZFH data presented in figure 4. At lower temperatures, $T_q \approx 35$ K, a number of anomalies in external electrical fields and in zero field [2, 8] mark the appearance of the `Müller state', the nature of which is still unclear, and different scenarios will be discussed below. At sufficiently low temperatures and for high enough fields an ordered polar state is induced. The field dependence of the transition into that state is well described by mean-field theory (the solid line in figure 13).

The topology of the phase diagram shown in figure 13 exhibits a striking similarity to various other cases. For example, for the relaxor ferroelectric PMN a similar E, T-diagram including paraelectric glassy and induced ferroelectric states has been published [42]. In this and related systems the cluster wall dynamics is thought to cause many of the interesting phenomena shown by these materials. In fact a pinned cluster state is also known to exist in Ca^{2+}-doped $SrTiO_3$, where the electrical field can be used to facilitate domain wall motion ([18], and references cited therein). Hence, the effect of impurities on the properties of nominally pure $SrTiO_3$ is debated and it has been conjectured that a polaronic mechanism

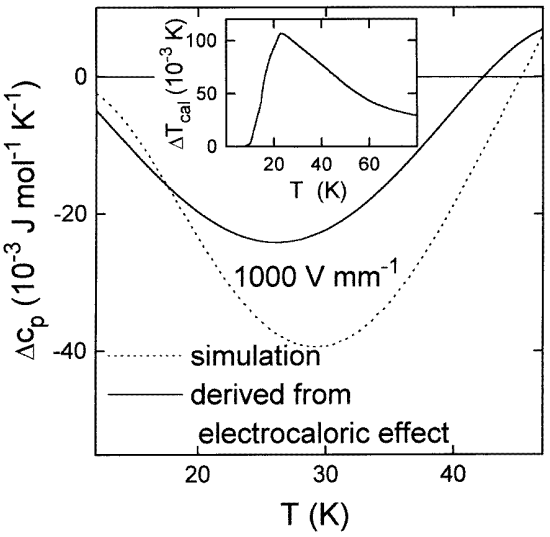

Figure 12. The temperature dependence of the field-dependent contribution of the specific heat. The solid line is an approximation based on measurements of the electrocaloric effect by Hegenbarth [17] shown in the inset. The dotted line was calculated using equations (10) and (11).

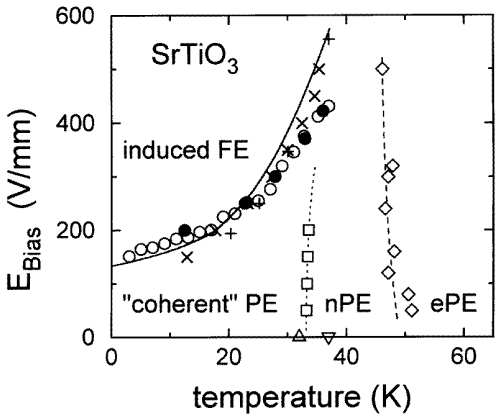

Figure 13. The E, T-phase diagram of $SrTiO_3$. Crosses ($\times$, this work; $+$, Hegenbarth [13]) represent the maxima occurring in $\varepsilon'(T)$. Full (●) and open (○) circles represent maxima in $\varepsilon''(T)$ and $\varepsilon''(E)$, respectively. The solid line has been calculated using the mean-field model, equation (1), and the averaged parameters as described in the text. The minima in $\chi_3(T)$ are indicated by open squares (□). The diamonds (◊) denote the significant change of slope in the thermoremanent polarization (see figure 4) separating the ergodic (ePE) and non-ergodic (nPE) paraelectric regimes. The EPR anomaly (▽: [2]) and the EXAFS anomaly (△: [8]) in zero field are also shown. The dashed and dotted lines are drawn to guide the eye.

[29] could cause the low-temperature relaxations observed in $SrTiO_3$ [9] and other incipient ferroelectrics.

The E, T-phase diagram of $SrTiO_3$ bears also some resemblance to the p, T-phase diagram of liquid He [43]. It is just this analogy with the case of the quantum fluid which

has led Müller and Tosatti to propose the existence of a macroscopic quantum state in $SrTiO_3$ [2]. The nature of this state is currently under intensive study and under controversial dispute. Several possible mechanisms aiming at explaining the unusual low-temperature properties are currently under discussion including quantum coherence and a polar cluster state. An experiment that looks likely to shed light on the Müller state seems to be the study of the wavelike propagation of temperature. Recent Brillouin scattering experimental results are compatible with an interpretation in terms of second sound [4]. Although predicted to occur in ferroelectrics [44] this non-diffusive propagation of heat is rarely observed in solids due the ubiquitous presence of defects leading to unwanted scattering of the longitudinal acoustic waves [45]. However, the propagation of second sound has been observed well above T_q and it is now generally believed that it cannot be a hallmark of the Müller state.

5. Summary

We have carried out a dielectric and calorimetric study of nominally pure (polydomain) $SrTiO_3$ samples with special emphasis on electric field effects at low temperatures. The dielectric constant as well as the contribution to the specific heat as measured in large dc fields can be analysed in terms of the transverse Ising model augmented by an electrical field term. This detailed analysis of the field-dependent dielectric constant provided indications for the existence of domains of dynamic origin. The deduced squared cluster polarization is compatible in magnitude with the order parameter deviations noted from EPR investigations [2]. This suggests that the cluster polarization measured in our experiments is closely connected to the order parameter of the state evolving below T_q.

Anomalies in the dielectric loss and in the FC/ZFH polarization were detected. Together with the dielectric constant data, these results were used to deduce a complex E, T-phase diagram. This diagram also contains the anomalies obtained at low fields detected in the third-order susceptibility measured at ac amplitudes 50 V mm^{-1} $< E <$ 450 V mm^{-1}. The anomalies in $\chi_3(E, T)$ at low fields were taken as evidence that FE correlations are suppressed by quantum fluctuations changing from incoherent to coherent quantum paraelectric behaviour. However, the heat capacity measurements demonstrate that there exists no conventional phase transition with a measurable anomaly in $c_p(T)$. In zero field, as well as in electrical fields up to 500 V mm^{-1} the specific heat reveals extra contributions below 10 K which remain unexplained so far but may correspond to low-lying excitations in the Müller state.

Acknowledgments

We would like to thank S Weinbruch and S Riedel for performing the electron microprobe measurements. Stimulating discussions with R Martoňák are acknowledged. We are grateful to E Courtens, R Martoňák and E Tosatti for supplying us with experimental and theoretical results prior to publication.

References

[1] Müller K A and Burkhard H 1979 *Phys. Rev.* B **19** 3593
[2] Müller K A, Berlinger W and Tosatti E 1991 *Z. Phys.* B **48** 277
[3] Vacher R, Pelous J, Hennion B, Coddens G, Courtens E and Müller K A 1992 *Europhys. Lett.* **17** 45
[4] Hehlen B, Péron A-L, Courtens E and Vacher R 1995 *Phys. Rev. Lett.* **75** 2416
[5] Courtens E, Coddens G, Hennion B, Hehlen B, Pelous J and Vacher R 1993 *Phys. Scr.* T **49** 430

[6] Balashova E V, Lemanov V V, Kunze R, Martin G and Weihnacht M 1995 *Solid State Commun.* **94** 17
[7] Nes O M, Müller K A, Suzuki T and Fossheim F 1992 *Europhys. Lett.* **19** 397
[8] Fischer M, Lahmar A, Maglione M, San Miguel M, Iti JP, Polian A and Bandelet F 1994 *Phys. Rev.* B **49** 12 451
[9] Viana R, Lunkenheimer P, Hemberger J, Böhmer R and Loidl A 1994 *Phys. Rev.* B **50** 601
[10] Bednorz J G and Müller K A 1984 *Phys. Rev. Lett.* **52** 2289
See also:
Bianchi U, Kleemann W and Bednorz J G 1994 *J. Phys.: Condens. Matter* **6** 1229
[11] Kleemann W and Schremmer H 1989 *Phys. Rev.* B **40** 7428
[12] Weaver H E 1959 *J. Phys. Chem. Solids* **11** 274
[13] Hegenbarth E 1964 *Phys. Status Solidi* **6** 333
[14] Hemberger J, Lunkenheimer P, Viana R, Böhmer R and Loidl A 1995 *Phys. Rev.* B **52** 13 159
[15] Uwe H and Sakudo T 1977 *Phys. Rev.* B **15** 337
[16] Barret J H 1952 *Phys. Rev.* **86** 118
[17] Hegenbarth E 1965 *Phys. Status Solidi* **8** 59
[18] Bianchi U, Dec J, Kleemann W and Bednorz J G 1995 *Phys. Rev.* B **51** 8737
[19] Blinc R and Žekš B 1974 *Soft Modes in Ferroelectrics and Antiferroelectrics* (Amsterdam: North-Holland)
[20] Böttcher C J F 1973 *Theory of Electric Polarization* vol 1 (Amsterdam: Elsevier)
[21] Sawyer C B and Tower C H 1929 *Phys. Rev.* B **35** 269
[22] Hemberger J 1994 *Diplomarbeit* Technische Hochschule Darmstadt
[23] Shirane G and Yamada Y 1969 *Phys. Rev.* **177** 858
[24] Mizaras R and Loidl A, unpublished
[25] See, e.g.,
Maglione M, Lopes dos Santos M, Chaves M R and Almeida A 1993 *Phys. Status Solidi* b **181** 73
[26] Dominik L A K and MacCrone R K 1994 *Phys. Rev.* **163** 756
[27] Doussineau P, Farsri Y, Frenois C, Levelest A, McEnany K, Toulouse J and Ziolkiewicz S 1993 *Phys. Rev. Lett.* **70** 96
[28] Lacroix R P and Béné G J 1951 *Arch. Sci.* **4** 430
[29] Bidault O, Maglione M, Actis M, Kchikech M and Salce B 1995 *Phys. Rev.* B **52** 4191
[30] Ruprecht G and Bell R O 1962 *Phys. Rev.* **125** 1915
[31] Migoni R, Bilz H and Bäuerle D 1976 *Phys. Rev.* B **17** 1155
[32] van der Klink J J, Rytz D, Borsa F and Höchli U T 1983 *Phys. Rev.* B **27** 89
[33] Levstik A, Filipic C, Kutnjak Z, Levstik I, Pirc R, Tadic B and Blinc R 1991 *Phys. Rev. Lett.* **66** 2368
[34] Feder J and Pytte E 1970 *Phys. Rev.* B **1** 4803
[35] Hehlen B, Kallassy Z and Courtens E 1996 *Ferroelectrics* at press
[36] This is extensively discussed in the literature on spin glasses and orientational glasses; e.g.
Binder K and Reger J D 1992 *Adv. Phys.* **41** 547
[37] Martoňák R and Tosatti E 1996 to be published
[38] Martoňák R and Tosatti E 1994 *Solid State Commun.* **92** 167
[39] Henning I and Hegenbarth E 1988 *Ferroelectrics* **79** 319
[40] Hegenbarth E 1962 *Phys. Status Solidi* **2** 1544
[41] Kikuchi A and Sawaguchi E 1964 *J. Phys. Soc. Japan* **19** 1497
[42] Colla E V, Koroleva E Yu, Okuneva N M and Vakhrushev S B 1995 *Phys. Rev. Lett.* **74** 1681
[43] Swenson C A 1950 *Phys. Rev.* **79** 626
[44] Gurevich V L and Tagantsev A K 1988 *Sov. Phys.–JETP* **67** 206
[45] Guyer R A and Krumhansl J A 1966 *Phys. Rev.* **148** 778